ELSEVIER

1 December 2000

Optics Communications 186 (2000) 155–166

OPTICS COMMUNICATIONS

www.elsevier.com/locate/optcom

Stability and bifurcations in Kerr-lens mode-locked Ti:sapphire lasers

M.G. Kovalsky *, A.A. Hnilo [1]

CEILAP, Centro de Investigaciones en Laseres y Aplicaciones (CITEFA-CONICET-UNSAM), Zufriategui 4380, 1603 Villa Martelli, Argentina

Received 27 June 2000; received in revised form 28 September 2000; accepted 29 September 2000

Abstract

Kerr-lens or self-mode-locked Ti:sapphire lasers are known to display several modes of operation, depending on the values taken by the system's parameters. The basic observed modes of operation are: continuous wave, mode locking with transform limited pulses, and mode locking with chirped pulses. These modes are naturally obtained from a description based on an iterative or Poincaré map of five pulse variables (beam size curvature, pulse duration, chirp and energy). The stability of these modes is obtained for an experimentally accessible range of the parameters. The theoretical predictions agree qualitatively with the experimental observations. For a particular bifurcation, we study the feasibility of an approximate description of the (five variables) dynamics with a one-variable map, which results in the logistic map.

Keywords: Nonlinear dynamics; Bifurcations and chaos; Ti:sapphire lasers; Mode locking

1. Introduction

The Ti:sapphire Kerr-lens mode-locked (KLM) laser has become the most widely used source of femtosecond (fs) pulses, but many of its dynamical properties remain poorly known. Physics of the KLM laser is intrinsically complex, because it is determined by a delicate balance of several spatial and temporal effects. In the temporal domain the group velocity dispersion (GVD) in all the optical components located inside the cavity and the intensity dependent self-phase modulation (SPM), mostly in the laser rod, are balanced by the dispersion produced by a pair of prisms. In the spatial domain, the relevant features are the laser cavity configuration and the intensity dependent self-focusing. The amplification is an additional source of nonlinearity, through gain saturation.

The usual approach is through some version of the master equation for passive mode locking [1]. This is, in general, an equation of the Ginzburg–Landau type [2], which has a vast (and quite unexplored) variety of dynamical behaviors. Partial or full numerical approaches can provide the values of the pulse variables, but the stability of the solutions is very difficult to obtain analytically.

The condition of stability against the appearance of satellite pulses has been computed by imposing conditions on the gain left after the pulse

* Corresponding author.

E-mail addresses: mkovalsky@citefa.gov.ar (M.G. Kovalsky), ahnilo@citefa.gov.ar (A.A. Hnilo).

[1] Investigador Adjunto, CONICET.

0030-4018/00/$ - see front matter
PII: S0030-4018(00)01032-4

passage [3,4]. Analyses of more general instabilities of the Ginzburg–Landau solutions (as, for example, pulse-to-pulse oscillations in the pulse duration) have been performed numerically [5]. Numerical approaches are powerful tools for laser design, but they provide a limited insight into the underlying dynamics, which is an interesting subject by itself. Besides, in obtaining the master equation, it is assumed that the pulse is slightly modified from one round trip to the next, an assumption that is observed to be not always valid outside the normal mode-locking stability range.

A standard approach to a complex nonlinear system reduces the study of the continuous time dynamics to the study of an associated discrete time system, the iterative, stroboscopic or Poincaré map [6]. A map is a sequence of values of the variables taken at discrete times. The description with maps is an alternative to that with a differential equation, and no information is gained or lost. There are, however, some immediate advantages: the dimensionality of the problem is reduced in (at least) one and the numerical simulations are easier and faster. However, most of the times, writing the map equation can be as difficult as solving the partial differential equation, unless the physical system has some "internal clock" that determines the position of the adequate discrete times. In the case of passive mode-locked lasers, that clock is provided by the cavity round trip time and, in fact, it is easy to obtain recursive equations linking the pulse variables in the $(n+1)$-round trip with the values taken at the n-round trip [7]. The stability of periodical solutions (as the mode-locking pulse train) is determined easily.

There are additional advantages when studying unstable behaviors i.e. there is no theoretical limitation on the acceptable pulse variation from one round trip to the next, and the observed period-doubled solutions [8–10] are trivially described with maps. Descriptions of the Ti:sapphire laser using maps have been developed to obtain the values of laser operation as well as their stability [7,11]. One of the predictions of this approach is the existence of instabilities that affect some, but not all of the pulse variables. This prediction has been experimentally verified recently [10].

In this paper, we go deeper into the map's approach to the Ti:sapphire KLM laser. We obtain not only the stability regions, but we also compute the unstable eigenvectors at the points where stability is lost (bifurcation points). We also try to describe the dynamics in the unstable region. In the Section 2 we briefly review the map's approach. In Section 3 we describe the different stable solutions obtained. The regions of stability are displayed, as well as the unstable eigenvectors. In the Section 4, the comparison with the observed dynamics is shown. In the Section 5, a simplified (one-dimensional) model is devised to get some intuitive insight into the dynamics close to one of the bifurcation points.

2. Approach to Ti:sapphire Kerr-lens mode-locked lasers using maps

At this point, we would like to warn that we do not ask our approach to provide a quantitative accurate prediction, but a qualitative accurate one. This is motivated by the extreme sensitivity of the system to noise and initial conditions, which makes an accurate numerical comparison hopeless. This situation is, in fact, common to practically all nonlinear systems outside the stability range. Instead, our hope is to unveil the most general and *structurally stable* [6] properties of the system. In simpler words, we do not care if the mode-locking operation loses stability at a GVD value of say -2000 fs^2 when it is predicted to do so at -1000 fs^2; instead we do care if it loses stability in the same *way*, for example, by period doubling the beam's spot size while the other pulse variables remain nearly constant. In consequence, at each step that some decision on the model is to be taken, we prefer the simplest choice that preserves the essential points (a presumably essential point, for example, is the functional dependence of the nonlinear coefficients on the pulse variables), rather than a more accurate, but also more complex, expression. Our goal here is not to design laser cavities, but to obtain a description that is as simple as possible, even at the cost of a poor quantitative agreement with experimental data, to

try to gain some nonnumerical insight into the KLM laser dynamics.

We start by supposing that the electric field inside the mode-locking pulse, as a function of the distance to the optical axis r and the time t, is given by:

$$E(t) = E_0 \exp(-ikr^2/2q) \exp(-ikt^2/2p) \tag{1}$$

where p, q:

$$\frac{1}{q} = \frac{n}{R} - i\frac{n\lambda}{\pi\sigma^2} \quad \text{and} \quad \frac{1}{p} = Q - i\frac{n\lambda}{\pi\tau^2} \tag{2}$$

are functions of the pulse variables: the spot radius σ, the beam curvature radius R, the pulse duration τ and the chirp Q (there is also a fifth pulse variable, the energy U, see later). As the pulse propagates through an optical element or distance, the p and q parameters change according to:

$$q_{\text{out}} = (Aq_{\text{in}} + B)/(Cq_{\text{in}} + D) \tag{3}$$

where $\{A \ldots D\}$ are the elements of a 2×2 matrix [12]. The same holds for p [13,14]. The matrix describing the effect of several elements is obtained by multiplying the matrices of each element. In general, the propagation is fully described by 4×4 matrices. In this way, it is easy to obtain the matrix that describes the effect of a round trip inside the laser cavity (Fig. 1). In the case of Ti:sapphire lasers, the Gaussian approximation (1) is valid for pulses longer than 10 fs [14], and, under appropriate design conditions [13] (which usually hold for Ti:sapphire laser cavities) the general 4×4 round trip matrix can be split into two diagonal blocks of 2×2. Therefore, the effect of a round trip on the parameters p, q can be described with a matrix of the form:

$$M = \begin{pmatrix} A & B & 0 & 0 \\ C & D & 0 & 0 \\ 0 & 0 & K & I \\ 0 & 0 & J & L \end{pmatrix} \tag{4}$$

The nonlinearity arises from the fact that the matrix elements include terms (due to the self-focusing and SPM in the laser rod) which are functions of the pulse variables. These terms, named here *nonlinearities* have the general form:

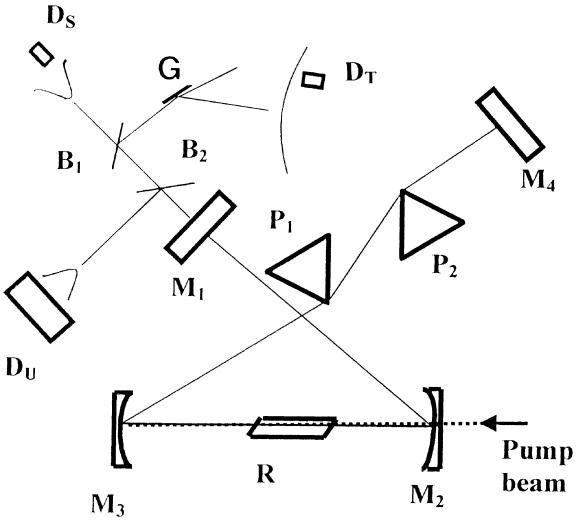

Fig. 1. Schematic of the laser and the measuring setup. M_1: 10% output coupler. M_2, M_3: focusing mirrors ($f = 50$ mm). M_4: rear mirror. R: Ti:sapphire rod ($L = 4$ mm). P_1, P_2: pair of prisms for GVD adjustment. The distances are (in mm): M_1–M_2 variable between 550 and 873, M_3–$M_4 = 1060$, M_2–$R = 51.5$, M_3–$R = 51.5$, P_1–$P_2 = 800$. B_1, B_2: beam splitters, G: diffraction grating (1200 mm^{-1}). D_U: photodiode probing the total pulse energy. D_S: photodiode probing the spot size. D_T: photodiode probing the spectrum. The intensity profiles of the pulse shape and spectrum are sketched.

$$\gamma = c_\gamma \frac{U}{\tau\sigma^4} \tag{5}$$

for the matrix elements $ABCD$, and:

$$\beta = c_\beta \frac{U}{\sigma^2\tau^3} \tag{6}$$

for the matrix elements $IKJL$. The constants c_γ, c_β are proportional to the nonlinear index of refraction of the Ti:sapphire. The complete expression of the nonlinearities as functions of the pulse's parameters is not trivial [15]. Here we use the "map E" definition, in the nomenclature of that reference. Its distinctive feature is that the nonlinearity is assumed to be effective over the Rayleigh length, rather than the entire rod's length, and that the value of the Rayleigh's length is calculated for the continuous wave (zero nonlinearity) case. This "map" is the one that reproduces best the stability regions observed.

It is convenient to define new variables: $S = \sigma^{-2}$, $T = \tau^{-2}$, $\rho = R^{-1}$. The expressions that link

the variable values at the $(n+1)$-round trip with the ones at the n-round trip are then:

$$S_{n+1} = \frac{S_n}{(A + B\rho_n)^2 + (B\lambda S_n)^2} \tag{7a}$$

$$\rho_{n+1} = \frac{(A + B\rho_n)(C + D\rho_n) + BD(\lambda S_n)^2}{(A + B\rho_n)^2 + (B\lambda S_n)^2} \tag{7b}$$

$$T_{n+1} = \frac{T_n}{(K + IQ_n)^2 + \left(\frac{IT_n}{\pi}\right)^2} = T_n \frac{L - IQ_{n+1}}{K + IQ_n} \tag{7c}$$

$$Q_{n+1} = \frac{(K + IQ_n)(J + LQ_n) + IL\left(\frac{T_n}{\pi}\right)^2}{(K + IQ_n)^2 + \left(\frac{IT_n}{\pi}\right)^2} \tag{7d}$$

The equation for the energy U is found by expansion of the usual equation of gain saturation for the mean values S^* and U^* [15] (note that there is a typing error in that reference):

$$U_{n+1} = U_n \left\{ 1 - \frac{2}{\mu} \left(\frac{U^* S_n + U_n S^*}{D_s} \right) + 4 \frac{\mu - 1}{\mu} \right\} \tag{7e}$$

where μ is the product of the small signal gain and the single passage feedback factor due to linear or passive losses (mirror's reflectivities, scattering, etc.), and $D_s = 1.22\ \mathrm{mJ\,cm^{-2}}$ is the saturation energy flux (i.e., the saturation energy multiplied by the cavity round trip) for Ti:sapphire.

The matrix elements in Eqs. (7a)–(7e) include the nonlinearities. It is convenient to express them as a series expansion:

$$A = A_0 + \gamma A_\gamma + \gamma' A'_\gamma + \gamma^2 A^{(2)}_\gamma + \gamma'^2 A'^{(2)}_\gamma + \gamma\gamma' A''^{(2)}_\gamma + \cdots \tag{8a}$$

the same for B, C, D, and:

$$K = 1 + 2\delta\beta' \tag{8b}$$

$$I = 2\delta \tag{8c}$$

$$J = 2\delta\beta\beta' + \beta + \beta' \tag{8d}$$

$$L = 1 + 2\delta\beta \tag{8e}$$

where 2δ is the value negative of the GVD per round trip. The coefficients of the expansions (8a) are only functions of the geometrical parameters. The factors γ and β are the nonlinearities, as defined by Eqs. (5) and (6), when the pulse crosses the rod from M_3 to M_2 (i.e., towards the output mirror). The factors γ' and β' are the nonlinearities when the pulse crosses the rod from M_2 to M_3.

The recursive relations (7a)–(7e) and (8a)–(8e) are the iterative map describing the laser dynamics. The operation values of the laser are obtained by imposing that the variables at the $(n+1)$-round trip are equal to the ones at the n-round trip. These are the *fixed points* of the map. The $\{A \ldots L\}$ elements include the nonlinearities which, in turn, are functions of the pulse variables. The general problem is intractable analytically. It can be solved in a closed way by assuming that only the first order in the nonlinearities is relevant. This is a good approximation for pulses longer than 10 fs, a limit we are anyway restricted because of the Gaussian pulse approximation (1). In this range, the values for the fixed points agree with those observed satisfactorily [7].

3. Fixed points' stability

The KLM Ti:sapphire laser is known to have three modes of operation: continuous wave (here named P_0), mode locking of transform limited pulses (here named P_1) and mode locking of chirped pulses (here named P_2). These three modes of operation correspond to three fixed points of the map (7a)–(7e). They have a direct physical description.

We follow the transformations of the pulse as it travels inside the cavity, starting at the output mirror M_1 (see Fig. 1). The solution P_1 (Fig. 2a) corresponds to a transform limited pulse at the output. When the pulse traverses the rod, it acquires positive chirp through SPM and GVD. The pair of prisms introduce negative GVD, so that the pulse almost arrives unchirped to M_4. A new passage through the prisms introduces additional negative GVD. When the pulse returns to the rod, it almost has the same duration than when it left the rod, but with a negative sign chirp. The GVD and SPM at the rod compensate the negative chirp so that the pulse is transform limited when it leaves

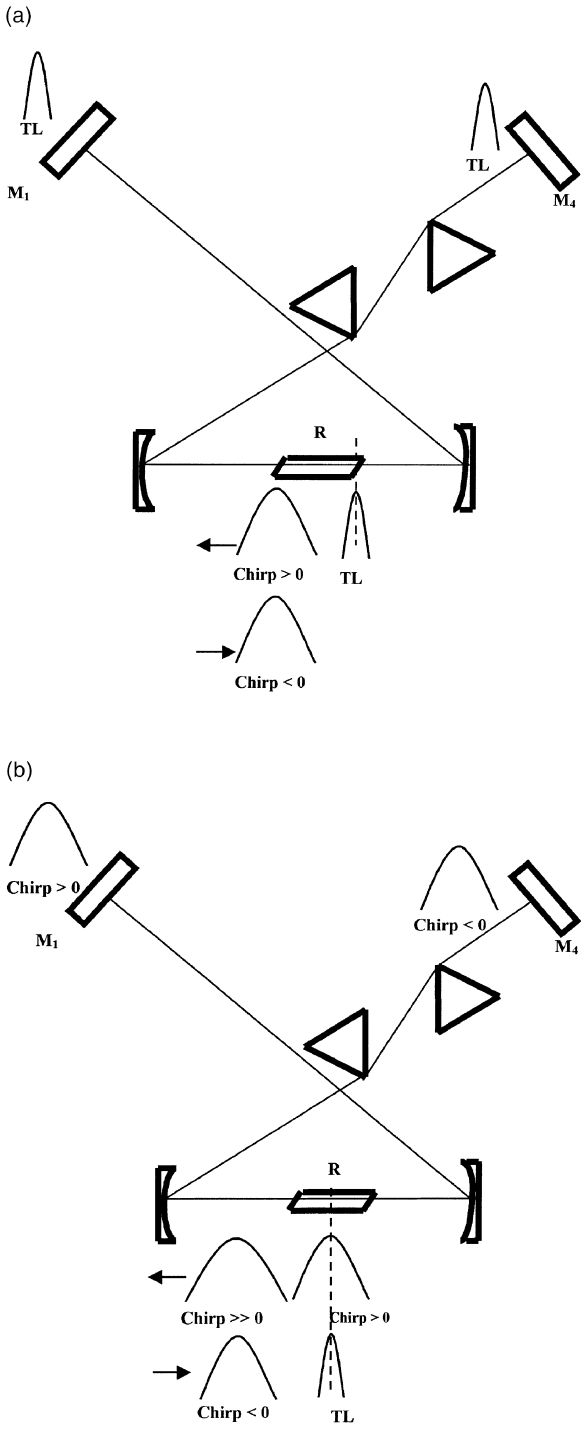

Fig. 2. Pulse chirp inside the cavity. The arrows indicate the propagation direction. The dashed line marks the plane of calculus. (a) mode P_1, (b) mode P_2.

the rod towards M_1, and the cycle is repeated. The calculation of the average nonlinear effects in the rod is difficult for the general case [7,15] but, from this simple picture, we see that, at the fixed point P_1, the nonlinear contribution when the pulse propagates towards M_1 is approximately the same that when it comes from M_1 (i.e., $\beta \approx \beta'$ and $\gamma \approx \gamma'$). This observation greatly simplifies the calculations.

The solution P_2 (Fig. 2b) corresponds to a chirped (positive) pulse at M_1. When it traverses the laser rod, it acquires more positive chirp and becomes longer. After two passages through the pair of prisms, it is negatively chirped enough to become transform limited at the center of the laser rod. Then it acquires some positive chirp in the remnant half of the rod, so that it arrives positively chirped at M_1, and the cycle is repeated. Note that inside the laser rod the pulse is (on average) much shorter when it propagates towards M_1 than when it comes from M_1, hence we can consider that the nonlinearities are significant when the pulse propagates towards the exit mirror only, i.e., we can approximate that $\beta + \beta' \approx \beta$ and $\gamma + \gamma' \approx \gamma$. Besides, the space and time foci are almost coincident, what allows a further simplification [16].

The fixed points can also be deduced from the examination of the second expressions (7c). One of the solutions is $T_n = T_{n+1} = 0$, which corresponds to P_0 (the continuous wave solution with $\tau \to \infty$). Otherwise, we have another solution with $Q_n = Q_{n+1} = Q^* = 0$, what implies $K = L$, $\beta = \beta'$, i.e., the P_1 solution (nearly equal nonlinearities in both directions and transform limited pulses). If $Q^* \neq 0$ instead, $2IQ^* = L - K$ and then $Q^* = \beta' - \beta$, which is positive, i.e., the P_2 solution. Then the pulse durations for P_1 and P_2 can be obtained from Eq. (7d) after some algebra.

In general, at the plane of the output mirror the solution P_2 has higher energy and longer pulses than P_1, and its region of stability is larger. The slope of the curve pulse duration vs. GVD (which is nearly a straight line in the usual GVD operation values) is twice larger for P_2 than for P_1.

One of the main advantages of the map's approach is that the stability of the operation modes of the laser is immediately calculated, by computing the eigenvalues of the Jacobian of the map

at the point of interest [7,15]. The fixed point is stable if the five eigenvalues have moduli smaller than 1. This analysis is complementary of the analysis of stability against satellite pulses.

In the following analysis we consider the stability regions and unstable eigenvectors only for the solution P_2, because it is the working point of the laser used in our observations. Stability plots for P_0 and P_1 can be found in Ref. [15]. The stability regions of P_2 are displayed in Fig. 3 as a function of two laser parameters: the negative GVD introduced by the intracavity pair of prisms and the crystal–output mirror distance named x. These parameters are chosen on account of their facility of access. The other laser parameters (distances, gain, etc.) are kept fixed. Their values are given in the figure captions, and they correspond to the laser used in the observations.

In the laser applications or design, we are interested in the determination of the regions of stable mode-locking operation. Here, instead, we are interested in the boundaries between the stable and the unstable regions. These boundaries are determined by the condition that at least one of the eigenvalues becomes equal to 1 (in modulus). Depending on the values of the parameters, the instability involves different eigenvalues and different associated eigenvectors (i.e., the directions in phase space, the fixed point becomes unstable). The calculated types of transitions, or bifurcations, are summarized in the Table 1. In the Fig. 3, these transitions are indicated with arrows (the dotted lines indicate the approximate position of the borders between transitions types). Transitions are classified in "verticals" if the unstable region is reached by moving only the x distance, and "horizontals" if the unstable region is reached by changing only the GVD.

Table 1
The predicted and observed types of transitions stable–unstable fixed point P_2, classified according to the main unstable direction of the respective eigenvector

Transition type	Eigenvalue	Main unstable variable
1A	+1	U
1B	+1	ρ, S
2A	−1	S
2B	−1	S, U
3A	c.c.	S
3B	c.c.	S, U

We found that the unstable eigenvectors have main components along one direction (type "A") or at most two (type "B") directions (in the five-

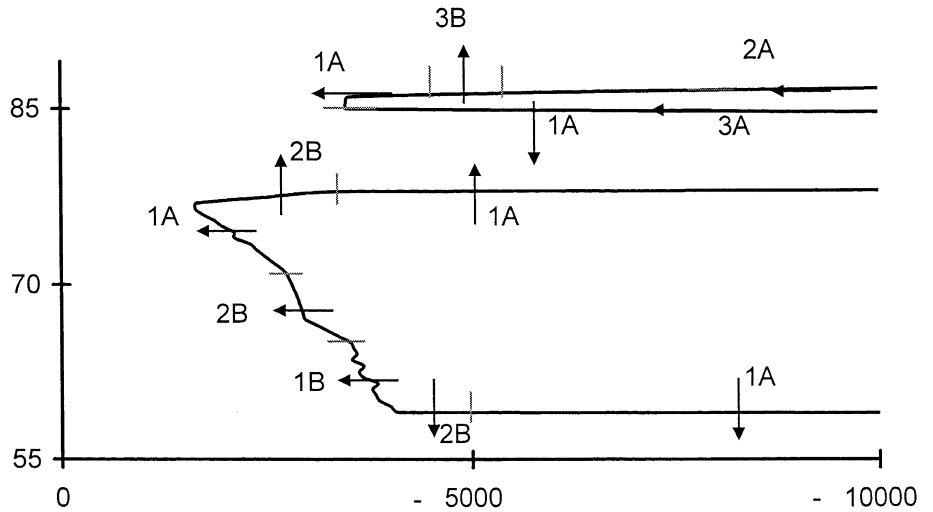

Fig. 3. Diagram of stability regions. There are two "islands" of stability in a surrounding region of instability. The arrows go from the stable to the unstable region and in each case the type of transition in indicated. The dotted lines indicate the approximate position of the borders between the transition types. Horizontal axis: prisms' GVD in fs^2. Vertical axis: x in cm.

dimensional phase space) parallel to the physical variables. For example, in the bifurcation type 1B, the normalized eigenvector has components: 0.766 in ρ, 0.642 in S and 10^{-9}, 10^{-10} and 10^{-9} in Q, T and U respectively. The low dimension of the unstable manifold is unexpected and it has important practical consequences, that is: the existence of "hidden" instabilities that can affect some of the pulse variables and are not detectable in the averaged signals (as the autocorrelation of the pulse) customarily used to test the mode-locking stability [10].

4. Experiments

The Ti:sapphire laser used in the observations is the seven-element design sketched in the Fig. 1. The output power is 300 mW for a 5W pumping (multiline Ar^+ laser). The minimum pulse duration is 66 fs, with the spectrum centered in 820 nm. In order to detect the selective nature of the instabilities, we prepare the following setup. The laser output goes through two beam splitters. One beam is collected by the photodiode D_U controlling the total pulse energy. This photodiode has a large area (1 cm^2), so that the whole laser spot is always collected. In order to detect pulse-to-pulse variations in the spot size, another beam is directed towards the photodiode D_S. It has an active region much smaller ($\varnothing$0.2 mm) than the spot size at that point ($\varnothing$2.5–5 mm), so that any pulse-to-pulse variation in the pump size is observable. Since there is no instrument capable of measuring pulse-to-pulse variations in the pulse duration or chirp in the fs range, we have to use an indirect method to measure the temporal variables. We assume that any modification in the pulse duration or chirp necessarily affects the pulse bandwidth (as it is the case of solitons). Therefore, the third beam is dispersed by a diffraction grating at near grazing incidence and a photodiode D_T is placed near one of the spectrum's edges, where the sensitivity to bandwidth fluctuations is presumably larger. We use the first diffracted order and place D_T ($\varnothing$0.2 mm) at 790 mm from the grating. We estimate that this setup has a spectral resolution of 0.25 nm.

In order to detect pulse-to-pulse variations confidently, the output of the photodiodes is recorded in the single sweep mode of a 400 MHz storage oscilloscope. In this way, we are able to detect variations in one of the pulse variables (for example, the spot size) even if the other pulse variables (for example, the energy) remain constant.

Starting from a regime of stable mode locking, we enter an unstable region by increasing (decreasing the absolute value) the (negative) prisms' GVD for a fixed value of $\underline{x}$. This is done by displacement of the pair of prisms (Fig. 1) along their axis of symmetry. We detect the unstable variables by inspection of the three photodiodes' traces. We repeat the procedure for different values of $\underline{x}$, and different types of instabilities, each of them involving different variables, are observed. We observed that the type of instability is the same inside a relatively small (see Fig. 3) range of values of $\underline{x}$.

We study in detail the four horizontal transitions. The vertical transitions access results unreliable because, when the $\underline{x}$ parameter is varied (i.e.: when the output mirror is displaced, even if it is mounted on a translation stage) the mode locking extinguishes. Some realignment is then required, altering so much the conditions that they become difficult to control. The number, relative position and type of all the observed transitions coincide with the predicted ones. In the following, we detail some selected illustrative examples.

With the output mirror in the farthest position we are able to obtain stable mode locking ($x = 86.5$ cm), the model predicts the 2A type transition as the GVD is increased, which should be observed as a period-doubling signal in the spot size, with negligible change in the other variables. This is precisely what is observed in Fig. 4a (period doubling in the spot size) and Fig. 4b (stable mode locking in the spectrum and hence in the pulse duration and the energy). We scan D_T through the spectrum, and at all positions the mode locking is constant, while D_S shows a stable period-doubled behavior. This observation is a striking confirmation of the predictions of the map's approach. Going deeper into the unstable region, Fig. 4c shows a tangent-like bifurcation. Note the small piece of almost stable mode locking at the

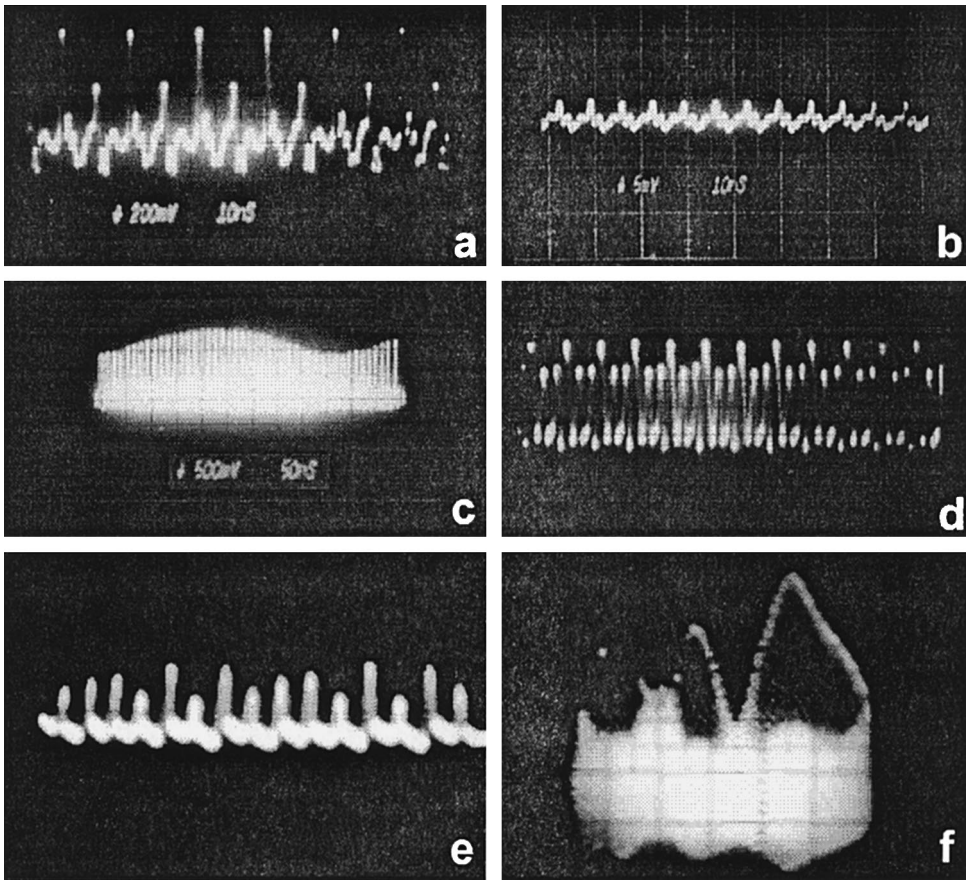

Fig. 4. Single-sweep traces showing: (a) the period doubling in spot size at $x = 86.5$ cm, (b) stable mode locking in the spectrum simultaneous with Fig. 3a, (c) a apparent tangent bifurcation in the spot size at $x = 86.5$ cm, (d) period three in the spot size at $x = 72$ cm, (e) period seven or chaos in the energy at $x = 72$ cm, (f) mode-locking and Q-switch near the position of 3e, Fig. 4a–d reproduced from Ref. [10].

beginning of the trace, and the nonperiodical wandering of the pulse height.

Then we reduce the value of $\underline{x}$. After a region where no stable mode locking can be obtained (in agreement with Fig. 3), a transition 1A is expected for $\underline{x} = 72$ cm. The instability here involves only the energy. A period three in the energy appears (Fig. 4d) while the other variables show stable mode locking. Going farther into the unstable region is observed a possibly chaotic output (period seven or more) in the energy (Fig. 4e) while the other variables still remain stable. It is worth mentioning that chaotic outputs are rare and difficult to record, for they destabilize to Q-switching (Fig. 4f) easily.

For $\underline{x} = 61$ cm the transition is predicted to be 1B, with the unstable direction having main components in the spot size and curvature variables. In agreement with this prediction, we find period doubling in the spot size (no change in the other probed variables). Since in this case the eigenvalues cross $+1$ in two variables, it is not obvious what behavior would be found. Numerical simulations of the complete (five variables) map show period-doubling behavior in the spot size, in agreement with the observations.

A word of warning is necessary in connection with the observations. It is assumed that the transversal laser mode is TEM_{00}, what must be carefully controlled at each step. Otherwise, one

may be confused by similar in appearance, but dynamically different spatio-temporal effects [8,9]. In order to ensure TEM_{00} operation, it is necessary to adjust the matching between the pumping laser beam and the Ti:sapphire oscillating mode. As the Ar^+ pumping laser mode presents thermal drifts, the matching must be periodically corrected by adjusting the position of the focusing lens. A too loosely focused beam allows the oscillation of transversal modes and it is observed to favor the appearance of satellite pulses. On the other hand, a too tight focusing inhibits the instabilities involving the spot size variable. In any case, a tight focusing makes our approximation of neglecting apertures untenable. We have taken care that each series of measurements has been performed with TEM_{00} mode and without the necessity of adjusting the focusing lens.

In summary, the theoretical predictions are verified, in the qualitative mode the approach is intended for. There are two experimental observations that deserve a special comment here. One is the existence of Q-switching instabilities in the close neighborhood of the chaotic regions. The other one is the well-known satellite pulse instabilities. Both phenomena can be included in the map's description by enlarging the map. In fact, the map (7a)–(7e) involves only the pulse variables, not the active medium variables. In particular, the saturated gain is not considered a dynamical variable, what is a strong simplification. This is done in order to obtain a description as simple as possible but, in view of the observed dynamics, it seems advisable to review that decision. On the other hand, adding another dimension implies calculating 36 partial derivatives and solving a sixth order polynomial for each point in the stable–unstable boundary. Fortunately, the experiments also indicate that the temporal variables play a secondary role i.e., they do not become unstable alone (see the Table 1) at least for the pulse duration range observed. So, to consider the pulse duration and chirp as slave variables results in a feasible simplification. In this way, a four-dimensional description (including the energy, the spatial variables and the gain) appears as a good way to try to improve the description without complicating the calculations.

5. One-dimensional map for the bifurcation 2A

Despite the many simplifications made, the description is so complex that it still heavily relies on numerical results. At a transition, however, only one or two variables are significant. We study the 2A transition at $\underline{x} = 86.5$ cm in more detail. We choose this transition because it is the only one (in the Table 1) that involves one single physical variable and an eigenvalue of -1, which is the case known to be advantageously described with maps. Due to the dominant role playing by the S variable (the unstable eigenvector is practically collinear with S), we build a one-variable map to attempt a simpler description of the dynamics at this point.

The other variables remain almost stable but they cannot be ignored. The variables U and ρ are the most relevant ones, so that we replace their values in the map by their expressions as functions of S. The variables Q and T, which variations are predicted to be even smaller, are replaced by their values at the fixed point. In this way (see the Appendix A) we obtain a one-variable map:

$$y_{n+1} = \frac{y_n}{\left[y_n^2 ab + c\right]^2 + \left[y_n d + y_n^3 ae\right]^2} \tag{9}$$

where $y_n \equiv S_n/S^*$. This map provides the value of the (inverse) beam area after one round trip, given the initial value of the beam area, the cavity design and the self-focusing parameter.

A nontrivial result is that the function (9) has a (single) extremum, i.e., there is one value of the beam area so that, in the next round trip, the area is minimal. As a consequence of the existence of an extremum, the map (11) is not invertible: there are, in general, two values of beam area that converge at the same value in the next round trip. This can be understood in the following way. A given value $\underline{A}$ of beam area can be reached, from the previous round trip, in two different ways. First, by "normal" propagation starting with some area A_l. Second, starting with a smaller area A_{nl}, that induces an intensity-dependent lens. For sufficient nonlinear strength, there is always some value A_{nl} that reaches $\underline{A}$ in the next round trip. It is not surprising that the extremum becomes more acute as the nonlinearity increases. Note that in the

absence of nonlinearity the beam area evolution is invertible (because the optical paths are invertible). The "non invertible" feature is at the basis of the existence of chaotic dynamics [17].

The stability of the fixed point is determined by the slope of the map at the fixed point (unstable if the derivative is larger than 1 in modulus). We insert the geometrical values of our laser and use the value of the net GVD (which determines the pulse duration) as a free parameter. As the GVD approaches to zero the pulse duration decreases and the nonlinearity increases. The slope at the fixed point at first increases almost up to the value $+1$ (but without reaching it), and then it decreases abruptly, crossing the value -1. This implies a period-doubling bifurcation, in agreement with the observation. This is easier to see by expanding Eq. (9) up to first order in the nonlinearity:

$$y_{n+1} = 4By_n\left(\frac{10ade + 3d^2}{8ade + 2d^2} - y_n\right) \tag{10}$$

where:

$$B = \frac{4ade + d^2}{2(2ade + d^2)} \tag{11}$$

The Eq. (10) is the logistic map for the variable y and the parameter B (which is a function of the net GVD per round trip). It is well known [17] that the logistic map exhibits a road to chaos via period doubling. An inverse cascade of period doublings, a period three stable window inside the chaotic region, and tangent bifurcations are also characteristic of this map (and are observed in our setup, see the Fig. 4). In particular, letting B_m the values of the parameter B at which the bifurcation from the 2^m to the 2^{m+1} cycle occurs, the bifurcations accumulate in such a way that:

$$\delta_m = \frac{B_m - B_{m-1}}{B_{m+1} - B_m} \tag{12}$$

converges, at the limit $m \to \infty$, to $\delta_m = 4.6692...$, a value which is called the Feigenbaum's constant (note: do not confuse δ_m with the net GVD per round trip parameter δ). This value is the same for all maps with quadratic extrema, regardless of their general shape. It is said then that all maps with a quadratic extremum belong to the same universality class [18]. The value of the limit (12) was found to be a function of the power degree of the extremum [19]. If a map of unknown features is given, the evaluation of the limit (12) is a good indicator that the unknown map belongs to the logistic map's universality class. In the case that we are studying here, the map (10) is obtained after a series of simplifications. The most uncertain one is the way the reduction of the dimensionality is performed. In order to estimate the error made, we calculate the bifurcations' diagram of the simplified map (10) (Fig. 5a) and of the complete five variables map (7a)–(7e) and (8a)–(8e), for the variable

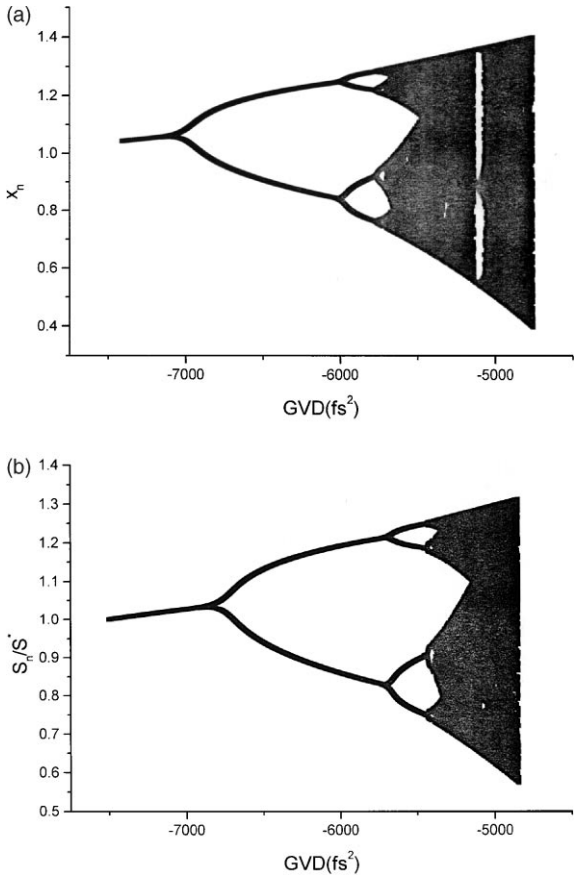

Fig. 5. (a) Diagram of bifurcations for the S variable (normalized with the fixed point value) calculated with the approximate one-dimensional map (10). (b) The same as (a), calculated with the complete (five-dimensional) map.

S (Fig. 5b) as a function of the net GVD in the cavity.

The diagram of Fig. 5a is, of course, the one of a logistic map (note the characteristic period three stable window near –5100 fs^2). The complete five variables map also displays a road to chaos via period doubling. The bifurcation points are slightly displaced (what is unimportant) and the period three stable window is absent. It is conceivable that the variations of the values of the other four variables, even if they are small, are capable to blur the period three stable window, without further consequences. But, what is more serious, the limit (12) converges at 4.980..., what indicates that the complete map does not belong to the logistic map's universality class. In other words, the simplified map (10) is a good approximation of the complete map only for the first few bifurcations. Well inside the chaotic region, the maps are essentially different. The simplified map (10) cannot be used confidently to describe the dynamics in the chaotic region. Anyway, as it was discussed before, it is presumable that the chaotic region cannot be described confidently even by the complete five variables map, for it is experimentally observed that chaotic signals tend to destabilize to Q-switching (what requires considering the gain as a sixth variable).

6. Summary

In this paper we have studied the KLM Ti:sapphire laser, not as a tool for observing ultrafast phenomena, but as an object of dynamical interest in itself. We have presented the results of an approach using a five variables iterative map. In this way, we have continued the research on this line initiated some time ago [7,15] and we have also detailed the way some theoretical predictions have been obtained, which have been experimentally confirmed recently [10]. The map's approach allows to explain the existence of the three observed operation modes of the Ti:sapphire laser easily. Not only the stability boundaries in parameter's space, but also the unstable eigenvectors, which give the main unstable directions in phase space, have been calculated and experimentally confirmed in a qualitative way. The resultant diagram results in a simple and qualitatively accurate picture of how the system becomes unstable, and is useful to detect hidden instabilities producing undesirable effects on almost any application.

Finally, we have studied in detail the instability named 2A. We have tried to obtain a simpler description, by building an approximate one-dimensional map for the only observed unstable variable S (the inverse of the spot area). The obtained map has resulted in the logistic map. This reduction of variables has allowed the intuitive understanding of the physics of the period-doubling destabilization mechanism and the approximate calculation of the first bifurcations. However, we have found that the complete and the reduced maps belong to different universality classes, and therefore, that the reduced map not necessarily provides an acceptable description of the dynamics in the chaotic region.

In conclusion, we have verified that the map's approach provides a satisfactory qualitative description of the Ti:sapphire laser at the instability points. Future steps on this line are: the addition of the population inversion as a dynamical variable in order to include the analysis of stability against satellite pulses and to describe the dynamics in the chaotic region (some of this has been done, from a different point of view, in Ref. [20]); and go deeper in the theoretical and experimental search of the reason of the ''inessential'' role played by the temporal variables observed (for pulses not shorter than 30 fs at least).

Acknowledgements

The authors thank Prof. O.E. Martínez and Prof. M.C. Marconi for their hospitality and helpful assistance during the performance of the experiments with the Ti:sapphire laser facility at the Laboratorio de Electrónica Cuántica (LEC), Facultad de Ciencias Exactas y Naturales, Universidad de Buenos Aires. We thank Ariel Libertun for a critical reading of the manuscript and Esther Ginieniewicz for correcting our English. This research was supported by the CONICET contracts PIP 0425/98 and 0638/98.

Appendix A. Map equation for the variable S

We replace:

$$A = A_0 + \gamma A_\gamma \tag{A.1}$$

$$B = B_0 + \gamma B_\gamma \tag{A.2}$$

in the expression (7a) and we substitute the fixed point for the energy variable in the expression of the nonlinearity (5) with the expression:

$$U^* = \frac{F}{S_0}(1 - H) \tag{A.3}$$

where S_0 is the value in the fixed point P_0. We define:

$$F \equiv D_s(\Gamma k^{1/2} - 1) \tag{A.4}$$

$$H \equiv \frac{F^2 c_\gamma c_\beta S_\gamma \pi^2}{\delta + p\pi^2 c_\beta F} \tag{A.5}$$

where S_γ is an algebraic function of the geometrical parameters of the cavity and p is a corrective factor that takes into account the finite amplifier's bandwidth [7]. The equation for the variable S takes the form:

$$S_{n+1} = \frac{S_n}{\left[a'b'S_n^2 + c'\right]^2 + \left[d'S_n + a'e'S_n^3\right]^2} \tag{A.6}$$

where:

$$a' = \frac{C_\gamma \frac{F}{S^*}}{\frac{\delta}{\pi C_\beta F} + p} \tag{A.7}$$

$$b' = A_\gamma + B_\gamma n\left(\rho_0 + \frac{\rho_0}{S_\gamma}\frac{H}{S^*}\right) \tag{A.8}$$

$$c' = A_0 + B_0 n\left(\rho_0 + \frac{\rho_0}{S_\gamma}\frac{H}{S^*}\right) \tag{A.9}$$

$$d' = B_0 n\frac{\lambda}{\pi} \tag{A.10}$$

$$e' = B_\gamma n\frac{\lambda}{\pi} \tag{A.11}$$

ρ_0 and ρ_γ are algebraic functions of the geometrical parameters of the cavity, n is the refraction index of the rod. We scale Eq. (A.6) with the expression of the S variable at the fixed point:

$$y_{n+1} \equiv \frac{S_{n+1}}{S^*}, \qquad a \equiv a'S^{*2}, \text{ etc.} \tag{A.12}$$

and the map (9) is obtained. The parameter a depends of the GVD value δ, while the others parameters are only functions of the geometric distances. The slope of the map as a function of a is:

$$y'_{n+1} = \frac{D(y_n) - y_n D'(y_n)}{[D(y_n)]^2} \tag{A.13}$$

where $D(y_n)$ is the denominator in Eq. (9). In the fixed point $y_n = 1$ and $D(y_n) = 1$ so that:

$$y'_{n+1} = 1 - D'(1) \tag{A.14}$$

Inserting now the values of the geometrical parameters, we see that as the parameter a grows, the slope of the map decreases being $y'_{n+1} = -1$ for $a = 0.7156$.

References

[1] O. Martínez, R. Fork, J. Gordon, J. Opt. Soc. Am. B 2 (1985) 753.
[2] H. Haus, J. Appl. Phys. 46 (1975) 3049.
[3] H. Haus, J.G. Fujimoto, E.P. Ippen, J. Opt. Soc. Am. B 8 (1991) 2068.
[4] J.L.A. Chilla, O.E. Martinez, J. Opt. Soc. Am. B 10 (1993) 638.
[5] C.J. Chen, P.K.A. Wai, C.R. Menyuk, Opt. Lett. 19 (1994) 198.
[6] S. Wiggins, Introduction to applied nonlinear and dynamical systems and chaos, Springer, New York, 1990.
[7] A.A. Hnilo, J. Opt. Soc. B 12 (1995) 4.
[8] D. Coté, H. van Driel, Opt. Lett. 23 (1998) 715.
[9] G. Sucha, S. Bolton, S. Weiss, D. Chemla, Opt. Lett. 20 (1995) 1794.
[10] M.G. Kovalsky, A.A. Hnilo, C.M.F.G. Inchauspe, Opt. Lett. 24 (1999) 1638.
[11] M.-D. Wei, W.-F. Hsieh, C.C. Sung, Opt. Commun. 155 (1998) 406.
[12] A. Siegman, Lasers University Science Books, Mill Valley, 1986.
[13] A.G. Kostenbauder, IEEE J. Quant. Electron. 26 (1990) 1148.
[14] O.E. Martínez, J.L.A. Chilla, Opt. Lett. 17 (1992) 17.
[15] M. Marioni, A. Hnilo, Opt. Commun. 147 (1998) 89.
[16] I.P. Christov, V.D. Stoev, M.M. Murnane, H.C. Kapteyn, Opt. Lett. 20 (1995) 2111.
[17] E. Ott, Am. Phys. Soc. 53 (1981) 655.
[18] R.V. Mendes, Phys. Lett. 84 (1981) 1.
[19] P. Hauser, C. Tsallis, E. Curado, Phys. Rev. A 30 (1984) 2074.
[20] J. Jasapara, W. Rudolph, V. Kalashnikov, D. Krimer, I. Poloyko, M. Lenzner, J. Opt. Soc. Am. B 17 (2000) 319.